Geophys. J. Int. (2004) **158,** 888–897 doi: 10.1111/j.1365-246X.2004.02358.x

Influence of magnetostatic interactions on first-order-reversal-curve (FORC) diagrams: a micromagnetic approach

Adrian Muxworthy,[1,*] David Heslop[2] and Wyn Williams[1]

[1] *Institute for Earth Sciences, University of Edinburgh, Edinburgh, UK*
[2] *Fachbereich Geowissenschaften, Universität Bremen, Bremen, Germany*

Accepted 2004 May 12. Received 2004 May 5; in original form 2004 March 2

SUMMARY

From experiments it is known that magnetostatic interactions between grains strongly affect the magnetic hysteresis behaviour of samples, however, because of the difficulty in predicting the non-linear behaviour, the effect of interactions has not yet been fully incorporated into theoretical models for the recently developed first-order-reversal-curve (FORC) method. For the FORC method to be widely used it is important to have such an understanding, for example, from a geological point of view there are many cases where interactions are known to be important, e.g. bacterial magnetosomes found in sedimentary rocks. Using a 3-D fast-Fourier transforms (FFT) micromagnetic model we have conducted a detailed study of the role of magnetostatic interactions on the FORC diagrams of assemblages of ideal single-domain (SD) magnetite-like grains. We have considered various anisotropies and the importance of the alignment configuration of the particle assemblages. We show that interactions can strongly affect the magnetic behaviour, for example, interacting assemblages of SD grains can display more MD-like FORC diagrams. Associating the FORC diagram with the Preisach diagram, we find that for moderate and weak interacting SD assemblages, the factorization interpretation of the Preisach diagram is correct, and in agreement with recent experimental results.

Key words: FORC diagram, hysteresis, magnetostatic interactions, micromagnetics, single domain.

1 INTRODUCTION

It is important to have a reliable method for characterizing the magnetic composition and grain size distribution of the magnetic minerals within geological samples, as the nature of these minerals strongly effect the magnetic signature. For example, the identification of the smallest magnetic grains containing only a single domain (SD) is important in absolute palaeointensity studies, as SD grains produce the most reliable results, whilst larger multidomain (MD) grains the least meaningful (Levi 1977). In palaeoclimatic studies information is often revealed by subtle changes in grain size distribution, as revealed by domain state, while the same grain size variations complicate the determination of relative palaeofield intensity from the same sediments (Lund & Schwartz 1999).

Determining the composition of the magnetic minerals of a rock is relatively straightforward, however, the identification of the domain state is more difficult. Conventional methods such as magnetic hysteresis are unfortunately sometimes ambiguous in characterizing natural rocks and sediments, because various combinations of mineral composition, grain size, internal stress and magnetostatic grain interactions can produce the same magnetic behaviour (e.g. Dunlop 2002; Muxworthy *et al.* 2003).

In an attempt to remove some of the ambiguity, Roberts *et al.* (2000) and Pike *et al.* (1999, 2001a,b) have developed a new method of mineral and domain state discrimination using a type of hysteresis curves called first-order-reversal-curves (FORCs) or first-order return branches (Mayergoyz 1986; Bertotti 1998). Constructing a FORC diagram requires lengthy measurements, which has only recently become possible with fast and sensitive vibrating-sample magnetometers and alternating-gradient magnetometers. Each FORC is measured by saturating the sample, decreasing the field to a value H_a, and reversing the field sweep to the saturated state in a series of field steps (H_b). This process is repeated for many values of H_a. The magnetization $M(H_a, H_b)$ is measured at each step and the mixed second derivative taken to give the FORC distribution (Roberts *et al.* 2000), which is also referred to as the Everett function (Everett 1955);

$$\rho(H_A, H_B) \equiv -\partial^2 M(H_A, H_B)/\partial H_A \partial H_B \quad (1)$$

To construct the FORC diagram, a quadratic surface is fitted over a local area defined by the smoothing factor (SF). The larger SF, the greater the number of points used. These surfaces are combined to

*Coresponding author: Adrian Muxworthy, School of GeoSciences, Grant Institute, University of Edinburgh, Kings Buildings, West Mains Road, Edinburgh, EH9 3JW. E-mail: adrian.muxworthy@ed.ac.uk

give a piecewise quadratic surface. When the distribution is plotted as a contour plot of $\rho\,(H_A, H_B)$, i.e. a FORC diagram, it is convenient to rotate axes by changing coordinates from $\{H_A, H_B\}$ to $\{H_C = (H_B - H_A)/2,\ H_U = (H_B + H_A)/2\}$.

The FORC method originated in the phenomenological Preisach–Néel theory of hysteresis (Preisach 1935; Néel 1954). There are obvious similarities between a Preisach and FORC distribution, however, as the FORC diagram is defined from a purely experimental procedure it is hence less restrictive. For example, classical Preisach theory assumes that the distribution is symmetric about the H_C-axis; the FORC method does not.

Both measured Preisach and FORC distributions are thought to be highly sensitive to magnetostatic interactions. As a starting point to understanding the contribution of interactions to the FORC diagram, it is simplest to consider Néel's interpretation of the Preisach diagram (with $a = H_A > 0$, $b = H_B < 0$). Néel (1954) showed that for interacting SD grains, H_C corresponds to the coercive field of each SD loop in the absence of interactions and that H_U is the local interaction field. It follows in a very simple interpretation that $\rho\,(H_A, H_B)$ can be factorized and ρ is simply a product of two independent distributions: the coercivity distribution $g(H_C)$ and the interaction field distribution $f(H_U)$ (Dunlop *et al.* 1990; Bertotti 1998). However, this over-simplified interpretation has met with only mixed success (e.g. Dunlop 1968; Dunlop *et al.* 1990; Hejda & Zelinka 1990).

The current understanding of the effect of magnetostatic interactions on FORC distributions is poor. This is not because interactions are thought to be insignificant, but because they are difficult to quantify experimentally and to incorporate theoretically into models. Unlike non-interacting uniform SD grains that can be very well explained by analytical theories (e.g. Stoner & Wohlfarth 1948; Néel 1949), the behaviour of non-uniform magnetic structures, i.e. interacting SD grains and larger grains [i.e. pseudo-single-domain (PSD) and MD], is non-linear making it more difficult to determine (Brown 1963). With the rapid advancement in computing power, it has become possible to directly model this non-linear behaviour by implementing the micromagnetic formalism of Brown (1963) to study magnetic phenomena (e.g. Williams & Dunlop 1995; Winklhofer *et al.* 1997; Muxworthy *et al.* 2003).

There have been two previous published attempts to model the effect of interactions on the FORC diagram. As a first-approximation Pike *et al.* (1999) considered a simple Stoner–Wohlfarth (SW) type assemblage of grains to calculate the contribution of interactions. They implemented a moving Preisach model, which accommodates non-linear interactions by a linear approximation and is only really applicable for weakly interacting assemblages. Pike *et al.* (1999) found that experimentally observed negative regions lying just below the main peak on the lower half of the FORC diagram can be generated by magnetostatic interactions. Stancu *et al.* (2003) used both micromagnetic and Preisach analysis to model the effect of interactions on assemblages of uniaxial SD grains. Their Preisach analysis showed that this negative region is correlated with the sign of the mean-field interactions. Their micromagnetic model for a 2-D array of interacting particles, found that this same negative region is also correlated with the spatial arrangement of the particles in the model.

In this paper the effects of interactions on cubic grains of SD magnetite and magnetite-like minerals are examined using a 3-D micromagnetic model. In addition to considering a 3-D array instead of a 2-D array as in the independent study of Stancu *et al.* (2003), we take a more systematic approach to the understanding of interactions on FORC diagrams. For example, we consider the effect of interactions on assemblages of identical grains, whereas Stancu *et al.* (2003) modelled only assemblages of grains with distributions of coercive field and grain size. They modelled only assemblages with distributions as they consider the FORC diagram to be essentially a statistical problem (Stancu private communication, 2003).

We examine the effects of interactions on several different types of assemblages: regularly spaced assemblages with both randomly orientated and aligned SD grains with both uniaxial and cubic anisotropy, assemblages with partially random spatial distributions with varying particle concentration and assemblages of non-identical SD grains. We have implemented the standard method of FORC diagram determination as described by Roberts *et al.* (2000), rather than the extended data set method recently described by Pike (2003) as a result of some as yet unresolved inconsistencies with this new method.

2 THE MICROMAGNETIC MODEL

The basic micromagnetic algorithm used in this paper was fully described by Wright *et al.* (1997). Each grain is represented by a simple cube, that is, each cube represents the averaged magnetization direction of many hundreds of atomic magnetic dipole moments, or simply each cube is an ideal SD grain. The orientation of each magnetic cube can vary in direction. The grain assemblage structure is calculated by minimizing the total magnetic energy $E_{\rm tot}$, which is the sum of magnetostatic energy E_d and the anisotropy $E_{\rm anis}$ (Brown 1963; Wright *et al.* 1997). E_d is calculated using fast-Fourier transforms (FFT); this type of micromagnetic model allows the high resolution needed to examine arrays of interacting grains. The over-all structure of the assemblage of grains is determined by minimizing $E_{\rm tot}$ by the conjugate-gradient method (CGM) to give a local energy minimum (LEM) for the assemblage. The calculation of the energy terms and the implementation of the FFT are exactly the same as in the work of Wright *et al.* (1997).

In the model, $E_d \propto$ the spontaneous magnetization M_S^2 and $E_{\rm anis} \propto$ the magnetocrystalline anisotropy K_1. Values for M_S and K_1 were taken for magnetite at room temperature from Pauthenet & Bochirol (1951) and Fletcher & O'Reilly (1974), respectively. The exclusion of thermal agitation means that even though our model conditions are set for a magnetite-like material at room temperature, we are effectively modelling at 0 K. The cubic anisotropy K_1 value of magnetite was used in both the uniaxial anisotropy and cubic anisotropy equations.

No magnetostrictive anisotropy was included in the model, because its contribution is insignificant for SD magnetite grains (Fabian *et al.* 1996). The SD grains in the study were assumed to be stress-free, i.e. no dislocations and no external stress, making the contribution from the magnetoelastic anisotropy zero. Using a micromagnetic CGM algorithm with the necessary model simplifications to determine critical phenomena like hysteresis is unlikely to produce coercivities or remanences that exactly match those observed. These simplifications do not alter the trends reported in this paper.

2.1 Interaction considerations

In an assemblage of grains each particle experiences, in addition to any external field, dipole fields generated by neighbouring particles (Dunlop & West 1969). The dipole field generated from a stable SD grain is relatively constant compared to the time it takes for an SD grain to grain to rotate in the field. This makes it possible

to treat such interactions as static (Spinu & Stancu 1998). Smaller superparamagnetic grains are unstable as a result of the influence of thermal agitation and the interaction field associated with such particles is not constant during the time it takes for a neighbouring interacting magnetic moment to flip.

In this paper, we consider only static interactions rather than dynamic interactions. Dynamic interactions are only important for grains near the blocking volume, which for magnetite at room temperature is ∼30 nm (Dunlop 1973).

2.2 Generation of random distributions

In the following models, random distributions are discussed. There are two aspects to this; how were the random numbers generated and how large does the sample size need to be to represent truly random behaviour? The random numbers were generated using the RANDOM function of the Intel IFC7.0 compiler, which, is an implementation of the pseudo-random number generator algorithm described by Park & Miller (1988). The sample size was varied between 64 and 8000 grains. Little variation in behaviour was found between assemblages of 216 and 8000 grains. A sample size of 1000 grains was chosen.

3 INTERACTIONS BETWEEN REGULARLY SPACED IDENTICAL SD PARTICLES

3.1 Uniaxial anisotropy

Simulated FORC diagrams for assemblages of 1000 SD grains ($10 \times 10 \times 10$ grid) with uniaxial magnetocrystalline anisotropy, both aligned (U-A) and randomly (U-R) distributed, were calculated using 100 FORCs. The U-A assemblage had its easy axis orientated within 5° of that of the field. We consider the effect of variations in interaction spacing d (the distance between grains divided by grain dimensions; not the distance from grain centre to grain centre).

In Fig. 1, calculated FORCs are shown for the U-A regime with interaction spacing $d = 5$, which has been shown to be effectively non-interacting (Muxworthy *et al.* 2003). The U-A assemblage displays square FORCs, which when plotted on a FORC diagram (Fig. 1b) gives a symmetrical single peak at $H_C \sim 38$ mT, which because a quadratic surface has been fitted to it has a finite size. The finite size depends on both SF and the number of FORCs measured (Roberts *et al.* 2000): the higher SF the larger the peak width, the higher the number of FORCs measured the smaller the peak width. This non-interacting assemblage effectively behaves as one grain.

The random assemblage with $d = 5$, produces an asymmetric FORC diagram (Fig. 2), which has three main features: first, there is a central peak at $H_C \sim 28$ mT, which is more elongated than the aligned assemblage (Fig. 1b); secondly, the main peak displays an asymmetric boomerang shape; thirdly, there is a negative region near the bottom left of the FORC diagram.

The central peak is a result of the switching of the magnetization from negative to positive values near $H_C \sim 28$ mT (H_{B_2} in Fig. 2). From a more mathematical point of view, the positive peak is associated with the increase in $\partial M/\partial H_B$ with decreasing H_A as highlighted in Fig. 2.

The origin of the negative region is related to sections of the FORC curves where $H_B < 0$. As illustrated in Fig. 2, at H_{B_1}, $\partial M/\partial H_B$ decreases with decreasing H_A giving rise to negative values for ρ (H_A, H_B). The decrease in $\partial M/\partial H_B$ with H_A is not as pronounced for $H_B < 0$ and consequently the negative region is significantly smaller than the large central peak near H_{B_2}.

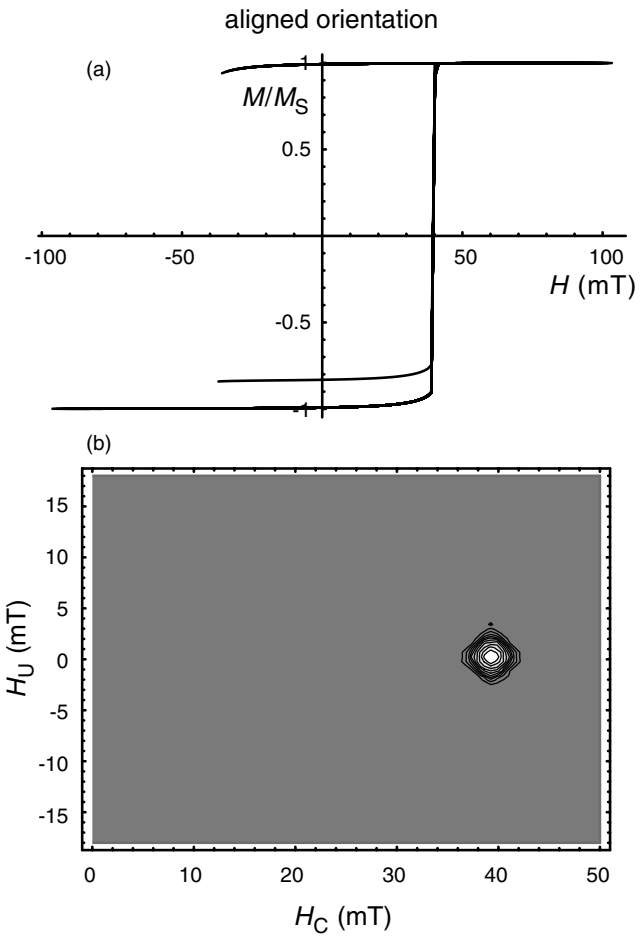

Figure 1. FORCs and FORC diagram for an assemblage of 1000 ideal single-domain (SD) grains with aligned uniaxial anisotropy with $d = 5$. In (b) a smoothing factor (SF) of 2 was used to fit the FORC distribution.

In Fig. 3, the raw FORCs shown in Fig. 2 are plotted in FORC space and the outline of the FORC diagram boomerang (Fig. 2) superimposed. It is clear that the boomerang shape is a result of the FORC algorithm picking out the contours in the raw data (Fig. 3). The lower left arm of the boomerang is related to FORCs near the relatively abrupt negative switching field. The right arm of the boomerang is related to more subtle contours, which are a result of the FORCs having different return paths as highlighted in Fig. 2. The shape of the return paths is controlled by the orientation of the grains with respect to the applied field, because the orientation controls the coercivity. Initially return curve behaviour are dominated by grains at ∼45° to the field. As H_A decreases, grains with orientations closer to 90° and 0° will start contributing to the hysteresis curve, so each time H_A is decreased the return path includes grains that have slightly different shapes of hysteresis loop. In other words, moving from the return path for a 45° assemblage in the first instance, into the return path for a randomly orientated assemblage. This effect is particularly enhanced for assemblage of identical grains.

The effect of varying the particle spacing on FORC diagrams for a U-A assemblage is shown in Fig. 4. As the interactions increase ($d \rightarrow 0$), the width of the peak in the H_U direction increases until $d \sim 1$ (Figs 4a and b), below which the well-defined peak disappears and FORC diagram becomes very noisy (Fig. 4c). The increase in the width of the peak is characterized by defining an interaction field H_i, which is the full-width-at-half-maximum (FWHM) of the

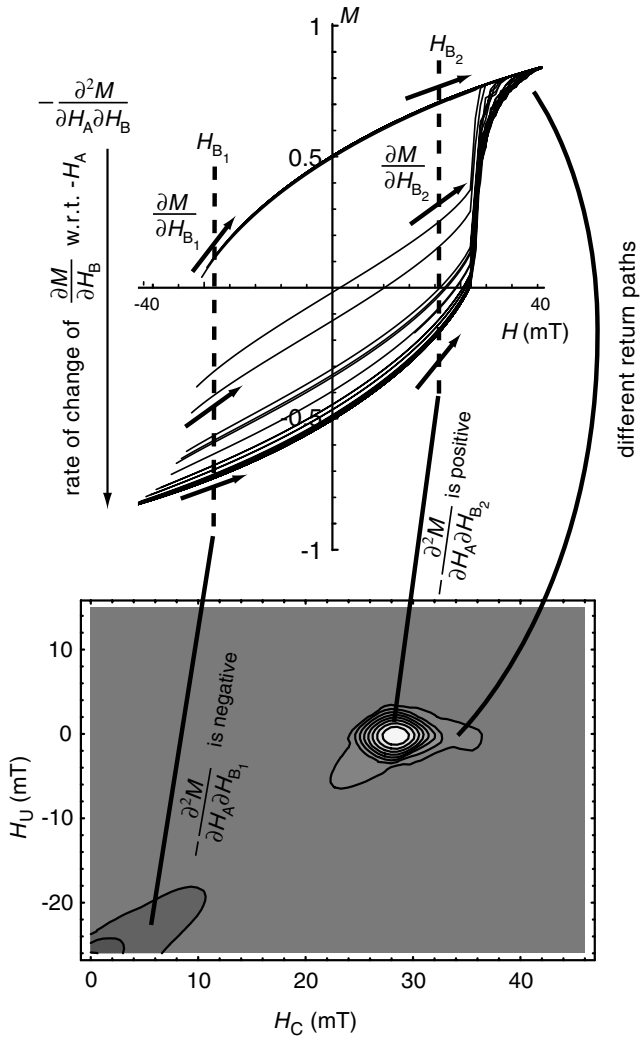

Figure 2. FORCs and FORC diagram for assemblages of 1000 ideal SD grains with randomly distributed uniaxial anisotropy with $d = 5$. For the FORC distribution SF = 4. The origins of the negative and positive regions in the FORC diagram are highlighted. The negative region is a result of a decrease in $\partial M/\partial H_B$ with decreasing H_A for negative values of $H_B(H_{B1})$. The large positive peak is associated with the increase in $\partial M/\partial H_B$ with decreasing H_A for positive values of H_B, near the switching field (H_{B_2}). The different return paths give rise to the positive region of the FORC distribution to the right of the main peak as illustrated. The origin of the boomerang shape is depicted in Fig. 3.

FORC distribution cut through the main peak in the H_U direction (Fig. 5a). H_i is plotted versus d in Fig. 5(b). H_i increases dramatically between $d \sim 2$ and $d \sim 1$, below which it is difficult to quantify. At $d = 5$, H_i is non-zero, which is due to fitting a quadratic surface to a delta surface (Fig. 1). For the purposes of comparison SF was kept constant in Fig. 5. The position of the main peak moves slightly towards lower H_C values with increasing interactions (Fig. 6).

The effect of interactions on the U-R regime is similar to that for the U-A one (*cf.* Figs 4 and 7); as d decreases, H_i increases sharply between $d \sim 2$ and $d \sim 1$, below which it is difficult to quantify (Fig. 5b). H_i increases less rapidly as $d \to 0$ for U-R than for U-A (Fig. 5b). There are other more subtle features. First, as the interactions increase, the boomerang shape seen in Fig. 2 becomes initially less defined and disappears. Secondly, the negative region near the H_U-axis for $H_U < 0$ becomes larger and more prominent and moves to larger values of H_U as well as further down the H_U-axis. As $d \to 0$ the magnetization of the assemblage becomes more reversible, more MD-like, however, for $d = 0$, i.e. touching SD grains, the appearance of the FORC diagram is noisy.

3.2 Cubic anisotropy (magnetite)

We directly model magnetite, that is, the uniaxial anisotropy modelled in Section 3.1 is replaced with cubic anisotropy (with $K_1 < 0$; eight easy directions).

An assemblage of non-interacting ($d = 5$) magnetite SD grains with aligned cubic anisotropy (C-A) produces a symmetrical FORC distribution that is a delta function. The corresponding FORC diagram is very similar in appearance to that shown in Fig. 1(b), but with a main peak at $H_C \sim 17$ mT. The field was applied within 2° of an easy axis. On decreasing d, the position of the main peak decreases along the H_C-axis (Figs 6 and 8) and H_i increases (Fig. 5b). For $d \sim 1$ the main peak splits symmetrically in two (Fig. 8c). This splitting is a result of the entire magnetic structure becoming temporarily trapped in intermediate states during partial hysteresis. As a result of the cubic anisotropy, each grain has eight easy directions, six of which are intermediate to the two easy directions the magnetization is switching between; three at 70.5° and three at 109° to the initial easy direction. It is these two sets of three easy directions and importantly that the grains have aligned anisotropy that cause the over-all domain structure to become temporarily trapped in intermediate states during hysteresis. This splitting is not seen in the U-A (Fig. 4), for the simple reason that the magnetocrystalline anisotropy does not have any intermediate stables. This splitting of the main peak is similar to the butterfly FORC diagrams found for assemblages of eight interacting elongated grains (Carvallo *et al.* 2003).

There are small negative regions similar to those seen for the U-R regime (Figs 2 and 7) in the lower-left of the FORC diagram.

As $d \to 0$ the FORCs display less hysteresis, i.e. less irreversible behaviour, however, similar to the U-A and U-R behaviour the FORC diagram becomes rather noisy. The butterfly distribution disappears as the effect of interactions starts to dominate over the magnetocrystalline anisotropy.

The randomly distributed, non-interacting ($d = 5$) cubic anisotropy regime (C-R) displays quite a different FORC distribution than the other non-interacting assemblages considered (Figs 1, 2 and 9). There is a main peak at $H_C \sim 11$ mT, but the peak is not closed, that is, it sweeps back on to the H_U-axis, similar to the type of FORC diagrams seen for small PSD magnetite crystals (Muxworthy & Dunlop 2002).

On decreasing d, again the position of the main peak decreases along the H_C-axis (Fig. 6) and H_i increases (Figs 5b and 9). As $d \to 0$ the raw FORCs are reversible, however, the FORC diagram becomes rather noisy.

This butterfly effect seen in Fig. 8(c) is not seen in the C-R assemblage, because there are many more intermediate stable states as a result of the random alignment of the anisotropy. The FORC distribution is spread out.

4 IRREGULAR ARRAYS OF GRAINS

It is possible to synthesize samples in the laboratory with crystals spaced on regular grids using methods like lithography (e.g. King

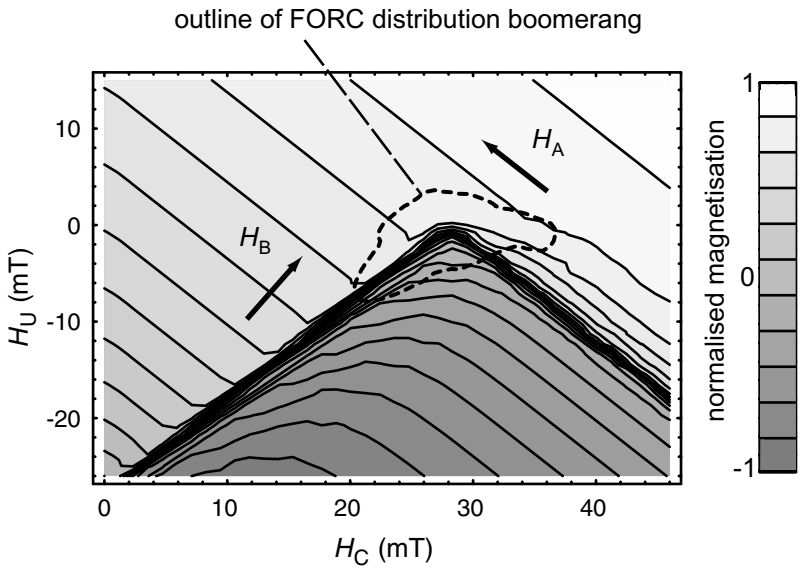

Figure 3. The raw data (FORCs) for randomly distributed uniaxial anisotropy with $d = 5$ plotted in FORC space. The FORCs are also shown in Fig. 2. The boomerang feature of the FORC distribution shown in Fig. 2 is superimposed on the raw data.

et al. 1996; Ross *et al.* 2002). However, in nature it is highly unlikely that magnetic grains will be evenly distributed, i.e. they are likely to be randomly distributed. The effect of random spacing on assemblages of identical grains with uniaxial and/or cubic anisotropy is considered.

Because an FFT algorithm was implemented to improve efficiency it was not possible with this algorithm to model a truly random distribution, as the algorithm requires that the cells are evenly distributed. However, it is possible to blank-out cells giving instead a discretized random distribution. For example if d is set to 1, then the possible spacings along a main coordinate direction are 1, 3, 6, etc., or if d is set to 0.5 then the corresponding spacings would be 0.5, 2, 3.5, etc. There is also a range of diagonal interaction spacings. This discretization is obviously only an approximation to a true random distribution, but it is thought that the same trends will still be displayed. Repeating the simulations for different randomly chosen spatial distributions yielded very similar FORC diagrams, suggesting that the results are for effectively random distributions. Note the value for d is now the minimum spacing not the absolute spacing as in Section 3.

We introduce a concentration parameter, which reflects the number of filled cells within the model; three concentrations of 10, 50 and 90 per cent were considered. A 100 per cent concentration was modelled in Section 3.

Increasing the concentration increases H_i (Fig. 10), in similar manner to decreasing d in Section 3. This is unsurprising, because by increasing the concentration we are effectively increasing the likelihood that a grain has another grain near it at the minimum interaction spacing. The general effect of concentration was independent on the type of anisotropy (uniaxial or cubic) and orientation (aligned or random). The negative region increased in size as the concentration increased.

Decreasing the minimum spacing d, has a very similar effect as decreasing the absolute spacing as in Section 3, that is, the FORC distribution becomes more MD-like in appearance as $d \rightarrow 0$. Again this effect was found to be consistent for both uniaxial and cubic anisotropies and both aligned and randomly orientated anisotropy.

5 DISTRIBUTIONS OF COERCIVE FIELD

Sections 3 and 4 considered assemblages of identical SD grains, which are unlikely to occur in nature, where grains usually have grain size and shape distributions that magnetically will lead to coercive-field distributions. These distributions are often, though not always, log-normally distributed (Kruiver *et al.* 2001; Heslop *et al.* 2002). In this section, we consider the effect of interactions on U-R assemblages of ideal SD grains with log-normally distributed H_C. To generate a distribution of H_C, for computation simplicity K_1 was varied rather than the grain volume, however, the net effect would be the same.

The mean of the log-normal distribution was that of $|K_1|$ for magnetite, i.e. 13.5 kJm^{-3}; only the width of the distribution was varied. Here, as in Section 3, the grains are distributed evenly on a grid with interaction spacing d.

The FORC diagram for a U-R non-interacting ($d = 5$) assemblage is strongly effected by variations in the log-normal distribution of the anisotropy; increasing the width of the distribution causes the FORC distribution to spread out along the H_C-axis (*cf.* Figs 2, 11a and b). The overall appearance is closer to that of experimental results on natural samples (e.g. Roberts *et al.* 2000; van Oorschot *et al.* 2002) than those for the single anisotropy models in Sections 3 and 4.

Decreasing d, i.e. increasing interactions (Fig. 11c), causes the FORC distribution to broaden in the H_U direction, i.e. H_i increases. The broadening is greater for low H_C values. This is because on average, the contribution of interactions to the assemblages magnetic behaviour is in direct competition with the anisotropy energy; the higher or harder the anisotropy the lesser the influence of the interactions on assemblage behaviour (Kneller 1969; Muxworthy *et al.* 2003). This effectively means that magnetostatic interactions will cause FORC distributions to broaden more significantly at low H_C values causing a uniform distribution to become more pear shaped.

The distinctive negative region of the FORC distribution is seen in the lower section of the FORC distribution in both the interacting and non-interacting assemblages (Fig. 11).

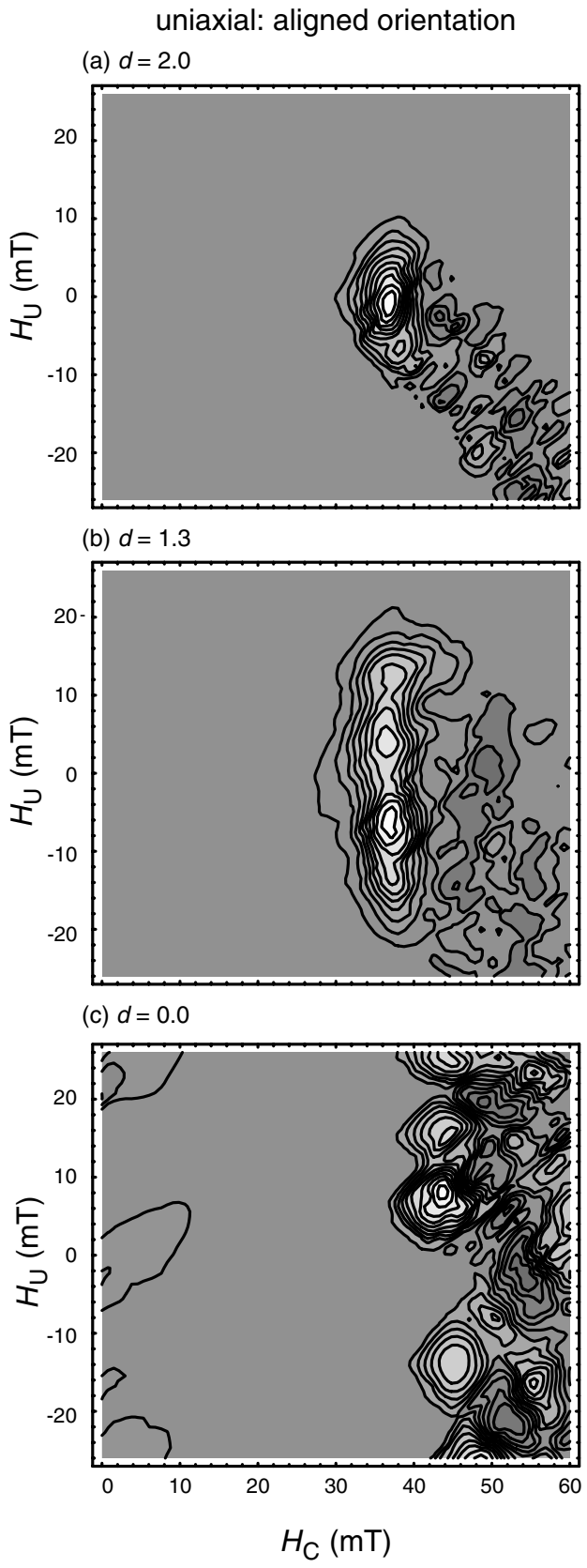

Figure 4. FORC diagrams for a U-A assemblage of 1000 ideal SD grains with different interaction spacings: (a) $d = 2.0$, (b) $d = 1.3$ and (c) $d = 0.0$. One of the two easy anisotropy directions of all the grains, is aligned with the field. In all three figures SF = 5.

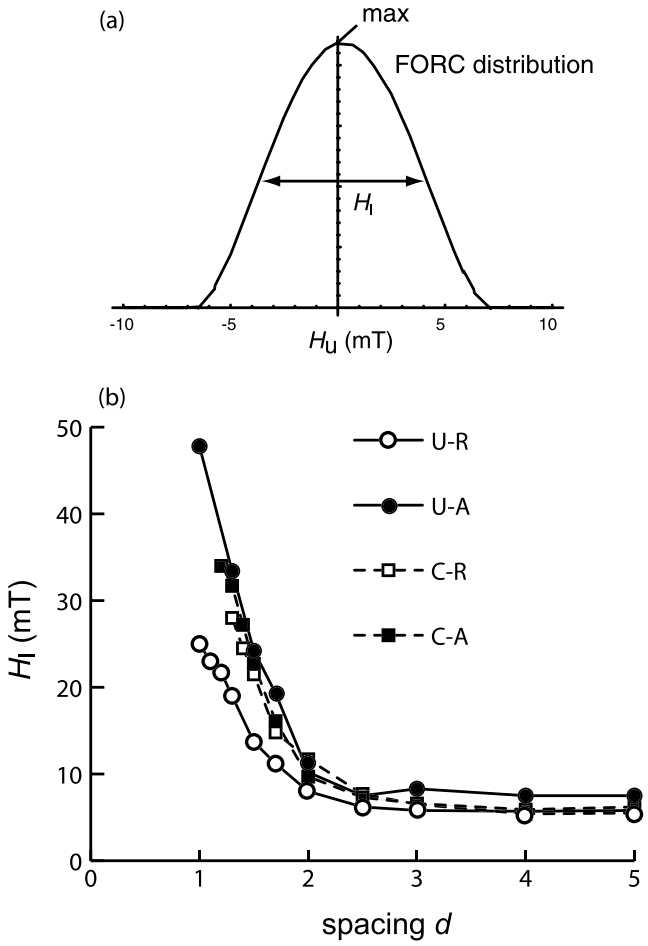

Figure 5. (a) Definition of H_I: FWHM of the main peak on the FORC distribution along the H_U direction and (b) H_i versus interactions spacing d for assemblages of ideal SD grains with uniaxial and cubic anisotropy, both aligned and randomly orientated. SF = 5 in all determinations of H_i.

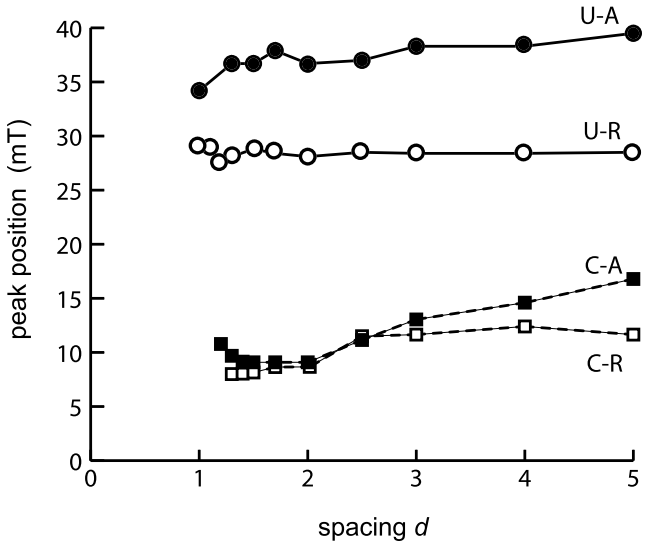

Figure 6. Position of main peak on the H_C-axis of a FORC diagram versus interaction spacing d, for assemblages of ideal SD grains with uniaxial and cubic anisotropy, both aligned and randomly orientated. SF = 5 in all determinations of peak position.

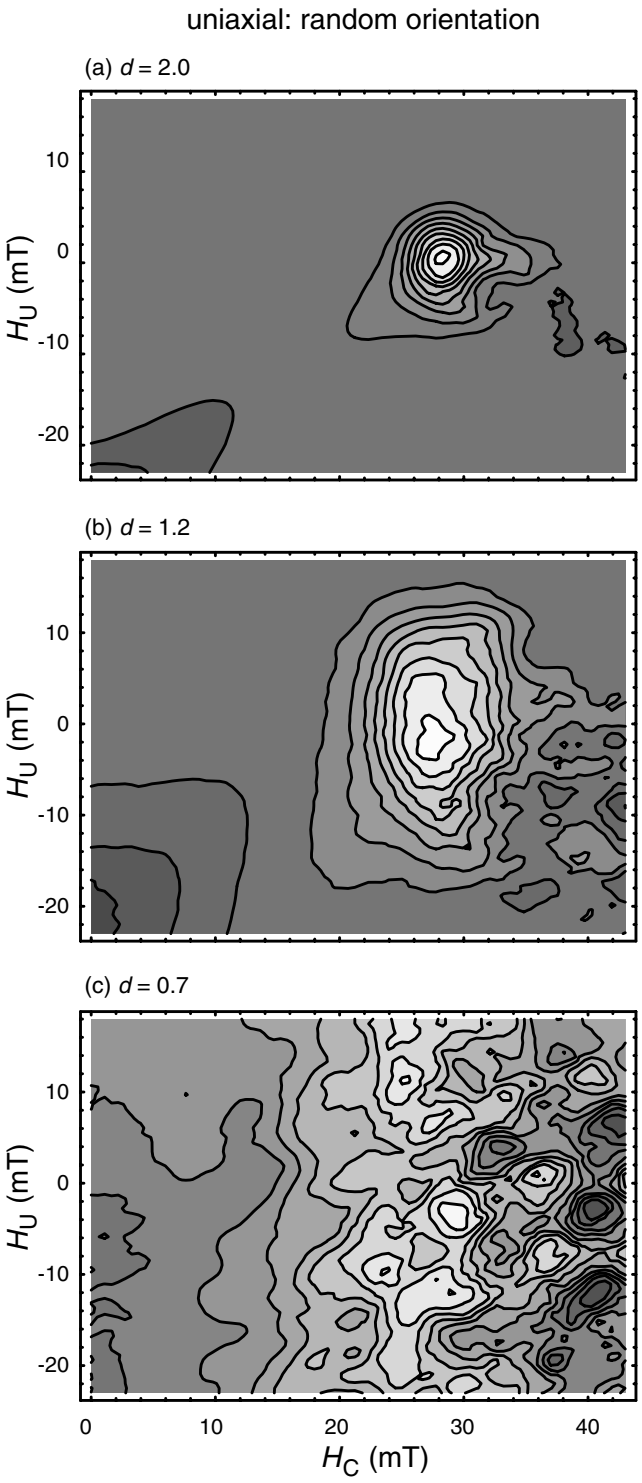

Figure 7. FORC diagrams for a U-R assemblage of 1000 ideal SD grains with different interaction spacings: (a) $d = 2.0$, (b) $= 1.3$ and (c) $d = 0.7$. In all three figures SF $= 5$.

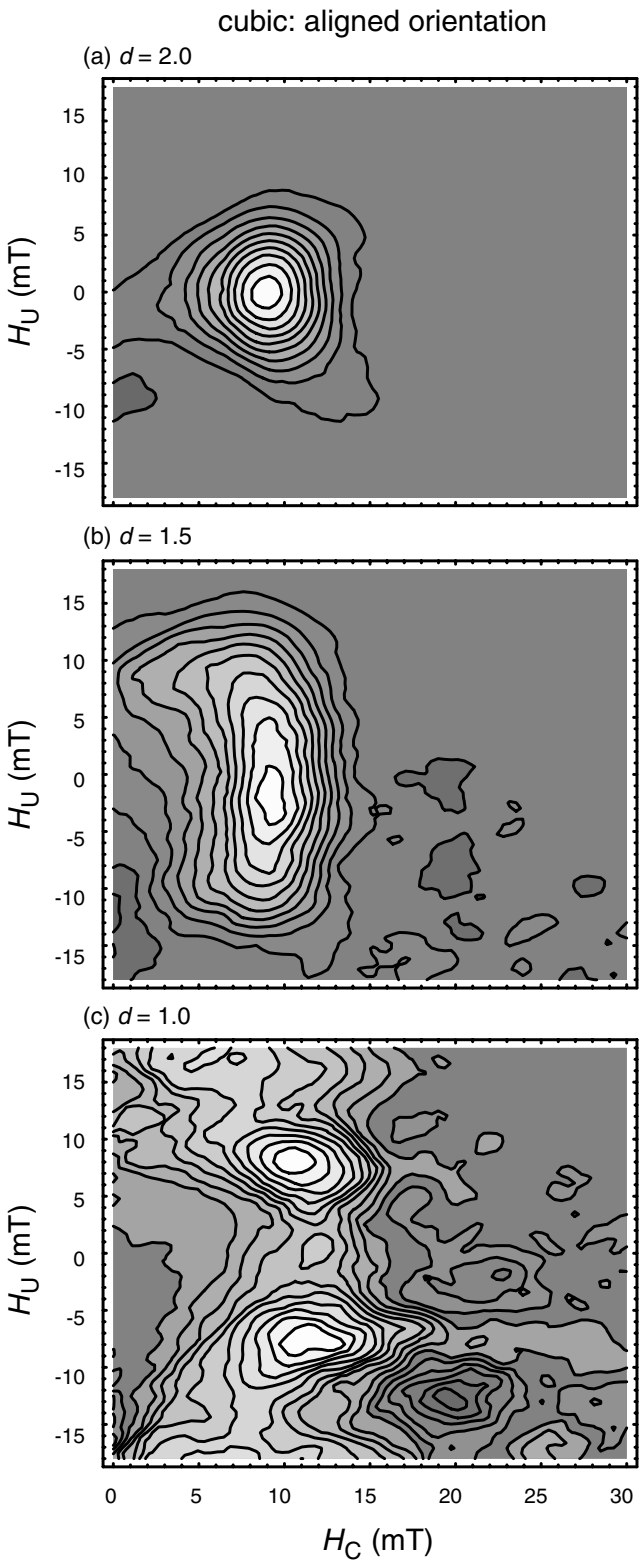

Figure 8. FORC diagrams for a C-A assemblage of 1000 ideal SD grains with different interaction spacings: (a) $d = 2.0$, (b) $= 1.5$ and (c) $d = 1.0$. One of the eight easy anisotropy directions is aligned with the field. In all three figures SF $= 5$. For $d = 5.0$ (not shown), the FORC distribution for the C-A regime is very similar to Fig. 1(b) and for $d = 0.0$ (not shown) it is similar to Fig. 4(c).

6 DISCUSSION AND CONCLUSIONS

The effect of interactions is clearly demonstrated in this paper. For assemblages of identical grains, certain consistent trends are seen regardless of the type of anisotropy or of the orientation of the grains: the effect of increasing interactions, i.e. decreasing d, is to cause the

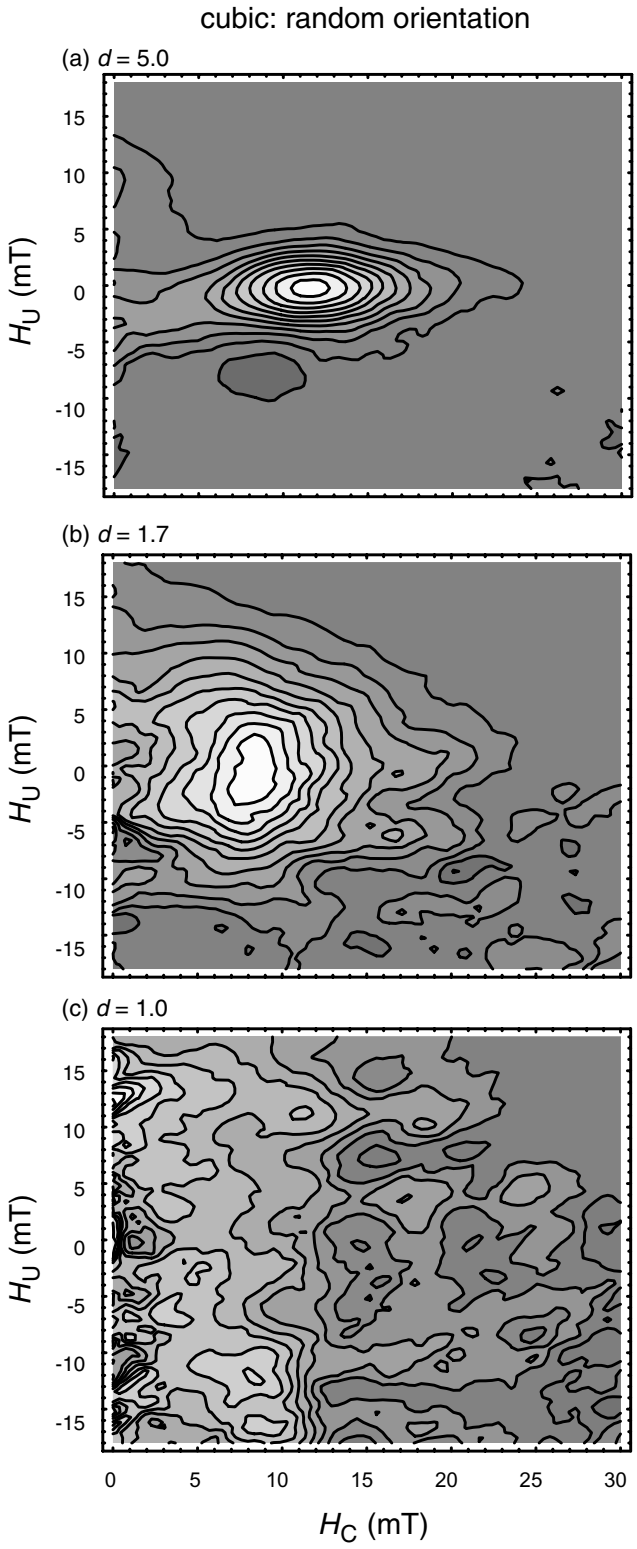

Figure 9. FORC diagrams for a C-R assemblage of ideal SD grains with different interaction spacings: (a) $d = 5.0$ (effectively non-interacting), (b) $d = 1.7$ and (c) $d = 1.0$. In (a), (b) and (c) SF = 5. For $d = 0.0$ (not shown), the FORC distribution for the C-R regime is very similar to Fig. 4(c).

main peak to spread in the H_U direction as d is decreased until $d \sim 1$, below which this peak collapses and spreads out. This part of the FORC distribution becomes noisy for $d < 1$. In addition, the main peak moves towards lower H_C values (Fig. 6),

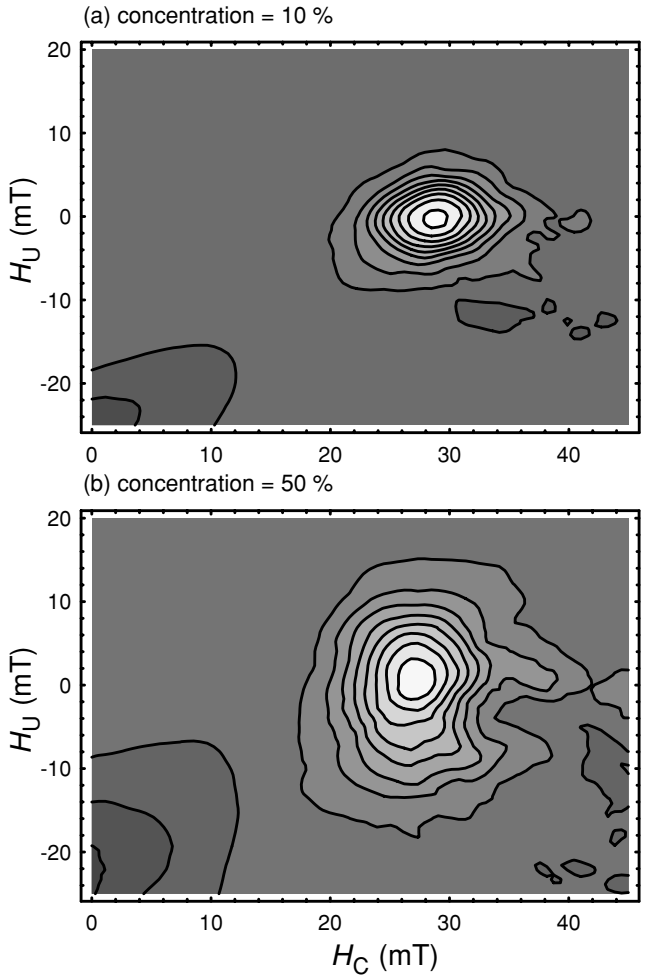

Figure 10. Effect of concentration on discretely randomized distributions (see text for explanation) of U-R SD grains: (a) 10 per cent concentration and (b) 50 per cent concentration. Minimum spacing $d = 1.0$.

though the reduction is quite small, especially for the uniaxial systems.

For $d > 1$, the factorization interpretation of the main peak of the FORC/Preisach diagram appears to be qualitatively correct, i.e. $\rho(H_A, H_B)$ is the product of two independent distributions: the coercivity distribution $g(H_C)$ and the interaction field distribution $f(H_U)$, in agreement with recent experimental findings for weakly interacting ($M_{RS}/M_S \sim 0.49$) elongated SD maghemite grains (Carvallo *et al.* 2004). However, it is realized that the slight decrease in the peak position with decreasing (Fig. 6) makes the factorization interpretation technically invalid.

One key feature that is repeatedly found in both theoretical and experimental FORC diagrams (this paper, Pike *et al.* 1999; Roberts *et al.* 2000; Pike *et al.* 2001a,b; Muxworthy & Dunlop 2002; van Oorschot *et al.* 2002; Carvallo *et al.* 2003; Stancu *et al.* 2003; Carvallo *et al.* 2004) is asymmetry. In particular, not just asymmetry but negative asymmetrical regions in the lower half of the FORC diagram (e.g. Fig. 11). There has been much debate about the origin of this asymmetry and of these negative regions. Both Pike *et al.* (1999) and Stancu *et al.* (2003) have suggested that the asymmetry is a result of interactions: Pike *et al.* (1999) found using a SW-type model, that interactions can produce asymmetry and negative regions in the lower half of the FORC diagram. However, to produce such negative regions, Stancu *et al.* (2003) showed with a 2-D

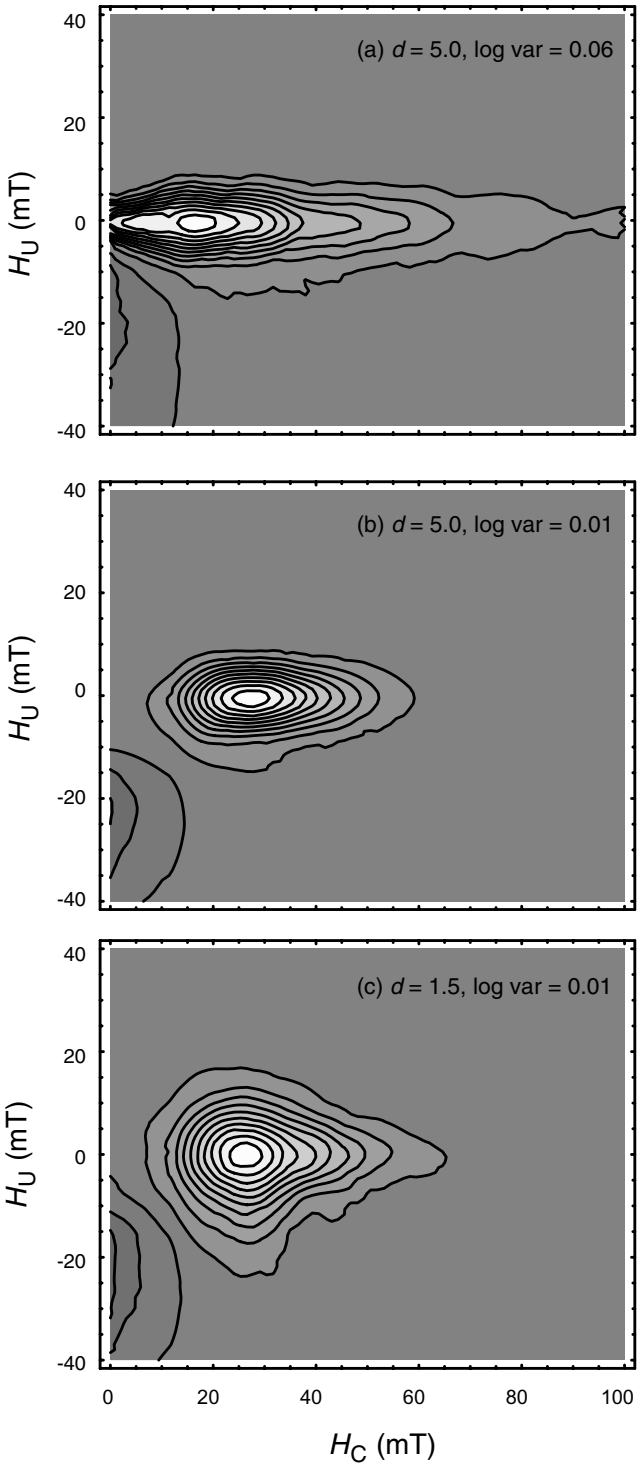

Figure 11. FORC diagrams for assemblages of SD grains with distributions of uniaxial anisotropy: (a) $d = 5.0$ (non-interacting), log variance $= 0.06$; (b) $d = 5.0$ (non-interacting), log variance $= 0.01$; and (c) $d = 1.5$, log variance $= 0.01$. The distribution in (a) is wider than that in (b) and (c).

micromagnetic model that asymmetrical regions in the lower half of the FORC diagram can be either positive or negative depending on the spatial distribution of the particles.

In this study, we found that the negative regions in the lower left area of the FORC diagrams are enhanced by interactions rather than due to them. These negative regions were more common in the U-R assemblage, but were also observed in the C-R and C-A assemblages. The origin of these negative regions is related simply to the shape of the FORCs as illustrated in Fig. 2. Negative regions are not observed for aligned anisotropy, because the FORCs are flat and there is no variation in $\partial M/\partial H_B$ with H_A. Small pockets of negative FORC distribution elsewhere on the FORC diagrams are the result of noise, which can be removed by increasing the SF.

When the random spatial distributions or the log-normal distributions of coercive field are examined, the interaction effects observed for assemblages of identical grains are less pronounced and smoothed. The inclusion of log-normal coercivity distributions (Fig. 11) causes the FORC distribution to spread out along the H_C-axis in agreement with other theoretical studies (e.g. Pike *et al.* 1999; Stancu *et al.* 2003).

What do the findings in this paper mean for the application of the FORC method to more general palaeomagnetic, rock and environmental magnetic investigations? Simply put, spreading of FORC diagrams at high coercivities can be assumed to be a result of the interactions between SD grains. Using such an interpretation of the FORC diagram may have many uses. For example, using FORC diagrams as a pre-selection technique in palaeointensity studies would be highly discriminative; the ideal sample would display a closed peak, little or no reversible magnetization and little or no spreading on the H_U direction. Clearly a hysteresis curve would be able to identify the ideal sample, but a FORC diagram would be better at distinguishing samples that are closer to ideal than hysteresis alone; hysteresis can not identify weak magnetic interactions. However, this would be a destructive pre-selection technique and would require sister samples.

ACKNOWLEDGMENTS

The authors have benefited from fruitful discussions with Chris Pike, Alexandur Stancu and Claire Carvallo, and constructive reviews from Lisa Tauxe and Andrew Newell. The work in Edinburgh was funded through NERC grant NER/A/S/2001/00539 to WW. DH is funded by the Research Centre Ocean Margins (RCOM), Universität Bremen.

REFERENCES

Bertotti, G., 1998. *Hysteresis in magnetism*, Academic Press, San Diego.

Brown, W.F., Jr, 1963. *Micromagnetics*, John Wiley, New York.

Carvallo, C., Muxworthy, A.R., Dunlop, D.J. & Williams, W., 2003. Micromagnetic modelling of first order reversal curve (FORC) diagrams for single-domain and pseudo-single-domain magnetite, *Earth planet. Sci. Lett.*, **213,** 375–390.

Carvallo, C., Özdemir, Ö. & Dunlop, D.J., 2004. First-order reversal curve (FORC) diagrams of elongated single-domain grains at high and low temperatures, *J. geophys. Res.,* **109,** 10.1029/2003JB002539.

Dunlop, D.J., 1968. Experimental test of the Preisach-Néel model of interacting single domain grains, *Phys. Lett.,* **27,** 617–618.

Dunlop, D.J., 1973. Superparamagnetic and single-domain threshold sizes in magnetite, *J. geophys. Res.,* **78,** 1780–1793.

Dunlop, D.J., 2002. Theory and application of the Day plot (M_{rs}/M_s versus H_{cr}/H_c) 1. Theoretical curves and tests using titanomagnetite data, *J. geophys. Res,* **107,** 10.1029/2001JB00486.

Dunlop, D.J. & West, G., 1969. An experimental evaluation of single-domain theories, *Rev. Geophys.,* **7,** 709–757.

Dunlop, D.J., Westcott-Lewis, M.F. & Bailey, M.E., 1990. Preisach diagrams and anhysteresis—Do they measure interactions?, *Phys. Earth planet. Int.,* **65,** 62–77.

Everett, D.H., 1955. A general approach to hysteresis: part 4—An alternative formulation of the domain model, *Trans. Faraday Soc.,* **50,** 1551–1557.

Fabian, K., Kirchner, A., Williams, W., Heider, F., Leibl, T. & Huber, A., 1996. Three-dimensional micromagnetic calculations for magnetite using FFT, *Geophys. J. Int.,* **124,** 89–104.

Fletcher, E.J. & O'Reilly, W., 1974. Contribution of Fe^{2+} ions to the magnetocrystalline anisotropy constant K_1 of $Fe_{3-x}Ti_xO_4 (0 < x < 0.1)$, *J. Phys.,*C., **7,** 171–178.

Hejda, P. & Zelinka, T., 1990. Modelling of hysteresis processes in magnetic rock samples using the Preisach diagram, *Phys. Earth planet. Int.,* **63,** 32–40.

Heslop, D., Dekkers, M.J., Kruiver, P.P. & van Oorschot, I.H.M., 2002. Analysis of isothermal remanent magnetization acquisition curves using the expectation-maximization algorithm, *Geophys. J. Int.,* **148,** 58–64.

King, J.G., Williams, W., Wilkinson, C.D.W., McVitie, S. & Chapman, J.N., 1996. Magnetic properties of magnetite arrays produced by the method of electron beam lithography, *Geophys. Res. Lett.,* **23,** 2847–2850.

Kneller, E., 1969. Fine particle theory, in *Magnetism and Metallurgy*, pp. 366–472, ed. Kneller, E., Academic Press, New York.

Kruiver, P.P., Dekkers, M.J. & Heslop, D., 2001. Quantification of magnetic coercivity components by the analysis of acquisition curves of isothermal remanent magnetisation, *Earth planet. Sci. Lett.,* **189,** 269–276.

Levi, S., 1977. The effect of magnetite particle size on paleointensity determinations of the geomagnetic field, *Phys. Earth planet. Int.,* **13,** 245–259.

Lund, S.P. & Schwartz, M., 1999. Environmental factors affecting geomagnetic field palaeointensity estimates from sediments, in *Quaternary climates, environments and magnetism*, pp. 323–351, ed. Thompson, R., Cambridge University Press, Cambridge.

Mayergoyz, I.D., 1986. Mathematical-Models of Hysteresis, *IEEE Trans. Mag.,* **22,** 603–608.

Muxworthy, A.R. & Dunlop, D.J., 2002. First-order reversal curve (FORC) diagrams for pseudo-single-domain magnetites at high temperature, *Earth planet. Sci. Lett.,* **203,** 369–382.

Muxworthy, A.R., Williams, W. & Virdee, D., 2003. The effect of magnetostatic interactions on the hysteresis parameters of single-domain and pseudo-single domain grains, *J. geophys. Res.,* **108** (B11), 2517, doi:10.1029/2003JB002588.

Néel, L., 1949. Théorie du traĭnage magnétique des ferromagnétiques en grains fins avec applications aux terres cuites, *Ann. Geophys.,* **5,** 99–136.

Néel, L., 1954. Remarques sur la théorie des propriétés magnétiques des substances dures, *App. Sci. Res.,* B., **4,** 13–24.

Park, S.K. & Miller, K.W., 1988. Random Number Generators: Good ones are hard to find, *Comm. A.C.M.,* **31,** 1192–1201.

Pauthenet, R. & Bochirol, L., 1951. Aimantation spontanée des ferrites, *J. Phys. Rad.,* **12,** 249–251.

Pike, C.R., 2003. FORC diagrams and reversible magnetization, *Phys. Rev. B,* **68**, 104424.

Pike, C.R., Roberts, A.P. & Verosub, K.L., 1999. Characterizing interactions in fine magnetic particle systems using first order reversal curves, *J. Appl. Phys.,* **85,** 6660–6667.

Pike, C.R., Roberts, A.P. & Verosub, K.L., 2001a. First-order reversal curve diagrams and thermal relaxation effects in magnetic particles, *Geophys. J. Int.,* **145,** 721–30.

Pike, C.R., Roberts, A.P., Dekkers, M.J. & Verosub, K.L., 2001b. An investigation of multi-domain hysteresis mechanisms using FORC diagrams, *Phys. Earth planet. Int.,* **126,** 11–25.

Preisach, F., 1935. Über die magnetische Nachwirkung, *Z. Phys.,* **94,** 277–302.

Roberts, A.P., Pike, C.R. & Verosub, K.L., 2000. First-order reversal curve diagrams: a new tool for characterizing the magnetic properties of natural samples, *J. geophys. Res.,* **105,** 28 461–28 475.

Ross, C.A. *et al.,* 2002. Magnetic behavior of lithographically patterned particle arrays (invited), *J. Appl. Phys.,* **91,** 6848–6853.

Spinu, L. & Stancu, A., 1998. Modelling magnetic relaxation phenomena in fine particles systems with a Preisach-Néel model, *J. Magn. Magn. Mater.*, **189,** 106–114.

Stancu, A., Pike, C.R. & Stoleriu, L., 2003. Micromagnetic and Preisach analysis of the First Order Reversal Curve (FORC) diagram, *J. Appl. Phys.,* **93,** 6620–6622.

Stoner, E.C. & Wohlfarth, E.P., 1948. A mechanism of magnetic hysteresis in heterogeneous alloys, *Phil. Trans. R. Soc. Lond.,* A., **240,** 599–602.

van Oorschot, I.H.M., Dekkers, M.J. & Havlicek, P., 2002. Selective dissolution of magnetic iron oxides with the acid- ammonium-oxalate/ferrous-iron extraction technique—II. Natural loess and palaeosol samples, *Geophys. J. Int.,* **149,** 106–117.

Williams, W. & Dunlop, D.J., 1995. Simulation of magnetic hysteresis in pseudo-single-domain grains of magnetite, *J. geophys. Res.,* **100,** 3859–3871.

Winklhofer, M., Fabian, K. & Heider, F., 1997. Magnetic blocking temperatures of magnetite calculated with a three-dimensional micromagnetic model, *J. geophys. Res.,* **102,** 22 695–22 709.

Wright, T.M., Williams, W. & Dunlop, D.J., 1997. An improved algorithm for micromagnetics, *J. geophys. Res.,* **102,** 12 085–12 094.